

# The influence of line opacity treatment in STELLA on supernova light curves

Alexandra Kozyreva<sup>1,2\*</sup>, Luke Shingles<sup>3</sup>, Alexey Mironov<sup>4</sup>  
 Petr Baklanov<sup>5,6,7</sup> Sergey Blinnikov<sup>4,5,6,8</sup>

<sup>1</sup>Max-Planck-Institut für Astrophysik, Garching bei München, 85748, Germany,

<sup>2</sup>Alexander von Humboldt Fellowship

<sup>3</sup>Astrophysics Research Centre, School of Mathematics and Physics, Queen’s University, Belfast BT7 1NN, UK

<sup>4</sup>Sternberg astronomical institute of Lomonosov Moscow State University, 119992, Moscow, Russia

<sup>5</sup>Space Research Institute (IKI), 84/32 Profsoyuznaya, Moscow, 117997, Russia

<sup>6</sup>NRC “Kurchatov Institute” – ITEP, Moscow, 117218, Russia

<sup>7</sup>National Research Nuclear University Moscow Engineering Physics Institute, Moscow, 115409, Russia

<sup>8</sup>Dukhov Automatics Research Institute (VNIIA), 127055 Moscow, 127055, Russia

Accepted XXX. Received YYY; in original form ZZZ

## ABSTRACT

We systematically explore the effect of the treatment of line opacity on supernova light curves. We find that it is important to consider line opacity for both scattering and absorption (i.e. thermalisation which mimics the effect of fluorescence.) We explore the impact of degree of thermalisation on three major types of supernovae: Type Ia, Type II-peculiar, and Type II-plateau. For that we use radiative transfer code STELLA and analyse broad-band light curves in the context of simulations done with the spectral synthesis code ARTIS and in the context a few examples of observed supernovae of each type. We found that the plausible range for the ratio between absorption and scattering in the radiation hydrodynamics code STELLA is (0.8-1):(0.2-0), i.e. the recommended thermalisation parameter is 0.9.

**Key words:** supernovae: general – supernovae – stars: massive – radiative transfer

## 1 MOTIVATION

Large sets of observational data have become available from supernova-search surveys and transient robotic systems. Among these data, there are dozens of discovered supernovae (SNe) with spectral snapshots spanning the earliest epochs up to hundreds of days after explosion. The comparison between observed spectral evolution of SNe and numerical simulations provides clues about the progenitor systems and the explosion mechanisms. One of the tasks for theoretical studies using radiative transfer simulations is to reproduce the evolution of the radiation field in the fast moving SN ejecta and the energy distribution across a wide spectral range. A number of sophisticated radiative transfer codes in the literature are used to carry out detailed spectral synthesis simulations (Mazzali & Lucy 1993; Baron et al. 1996a; Kasen et al. 2006; Dessart & Hillier 2010; Jerkstrand et al. 2011; Wollaeger et al. 2013, and many others). Other codes do not simulate spectra but assume approximate treatments for the formation of lines and the redistribu-

tion of energy resulting from radiation–matter interaction (Blinnikov et al. 1998; Bersten et al. 2011; Piro & Morozova 2014; Utrobin et al. 2015, and others).

In the current study, we discuss a particular aspect of radiative transfer simulations for SNe that reflects the micro-physics of photon–atom interaction, namely the probability for photons to be either resonantly scattered or inelastically absorbed. For the sophisticated codes from the first group, there is no simplification assumed. In the second group of codes, these processes are treated approximately with a thermalisation parameter that determines the ratio of scattering to absorption. In this paper, we discuss the best value to use for the thermalisation parameter in the hydrodynamics radiative transfer code STELLA by comparison to observed SNe and to advanced spectral synthesis codes.

In Table 1, we list several radiative transfer codes and their assumed values for the thermalisation parameter. Note that a few papers using SEDONA state different values of the thermalisation parameter, while the standard default value is  $\epsilon = 0.9$  for recent studies (Nathaniel Roth, Daniel Kasen, private communication). The choice of pure absorption line opacity can be justified on the basis that the strongest lines

\* E-mail: sasha@mpa-garching.mpg.de

**Table 1.** The choice of thermalisation parameter in different radiative transfer codes. Note, that [Baron et al. \(1996b\)](#) apply  $\varepsilon$  to a series of lines considered in LTE while doing full non-LTE radiative transfer. [Goldstein & Kasen \(2018\)](#) apply  $\varepsilon = 0$  for elements with atomic number  $Z \leq 20$ , and  $\varepsilon = 1$  for  $Z > 20$ . See text below for details about the choice of the thermalisation parameter in [Blinnikov et al. \(1998\)](#).

Reference	Absorption	Scattering	Code name	Application	Details
<a href="#">Baron et al. (1996b)</a>	0.05–0.1	0.9–0.95	PHOENIX	SNe Ia, II	Non-LTE with a number of LTE lines
<a href="#">Nugent et al. (1997)</a>	0.1	0.9	PHOENIX	SNe Ia	as above
<a href="#">Blinnikov et al. (1998)</a>	0/1	1/0	STELLA	SNe I, II	LTE; no temperature for radiation
<a href="#">Kromer &amp; Sim (2009)</a>	–	–	ARTIS	SNe I, II	
<a href="#">Dessart &amp; Hillier (2010)</a>	–	–	CMFGEN	SNe I, II	full Non-LTE from kinetic equations
<a href="#">Kasen et al. (2006)</a>	0.3–1	0.7–0	SEDONA	SNe Ia, II	LTE
<a href="#">Goldstein &amp; Kasen (2018)</a>	1/0	0/1	SEDONA	SNe Ia	as above
<a href="#">Shen et al. (2018)</a>	1	0	SEDONA	SNe Ia	as above
<a href="#">Utrobin et al. (2015)</a>	0	1	CRAB	SNe II	LTE with corrections for Non-LTE, grey atmosphere
<a href="#">Magee et al. (2018)</a>	0.9	0.1	TURTLES	early SNe Ia	LTE

are iron lines, and detailed studies (e.g. [Kasen 2006](#)) show that the iron lines are mostly purely absorptive. Although photons are not immediately thermalised, the true thermalisation timescale is extremely short ([Pinto & Eastman 2000](#)). Initial high-energy photons are absorbed and re-emitted at longer wavelengths, i.e. the effect of fluorescence occurs broadly in the SN ejecta (e.g. [Höflich 1995](#); [Lucy 1999](#); [Pinto & Eastman 2000](#)). [Goldstein & Kasen \(2018\)](#) suggest treating all lines from elements with atomic numbers below 20 ( $Z \leq 20$ ) as “purely scattering” and all lines from elements with atomic numbers above 20 as “purely absorptive”. [Kasen \(2006\)](#) analysed the effect of Ca II triplet on *I* band light curve and concluded that Ca must be treated as purely scattering, otherwise the *I* magnitude does not match observed light curves, in particular at the second maximum.

In the present study, we address the accuracy of line opacity treatment in the hydrodynamics radiative transfer code STELLA. In the basic descriptive paper about STELLA, the authors raised the issue of the choice between scattering and absorptive treatment of lines ([Blinnikov et al. 1998](#)). The STELLA light curves were compared to those calculated with EDDINGTON ([Eastman & Pinto 1993](#)), which is a full Non-LTE (no assumed Local Thermodynamic Equilibrium) radiative transfer code. Note that simulations with the LTE option and forced absorptive line opacity in EDDINGTON were used for that comparison analysis. [Blinnikov et al. \(1998\)](#) concluded that the lines in STELLA ought to be absorption-dominated in order to provide better agreement with EDDINGTON and with the observed SN 1993J. Hence, the standard value of thermalisation parameter in STELLA is  $\varepsilon = 1$  since 1998. More recently, STELLA is now the part of the latest MESA<sup>1</sup> release ([Paxton et al. 2018](#)) which is publicly available. STELLA operates under the assumption that thermalisation parameter is applied to all species, for all transitions, and independent of electron density, which is indeed a major simplification. However, the advantage of STELLA is that it is a hydrodynamics code, i.e., it solves implicitly coupled hydrodynamics and multigroup radiation transport. This enables STELLA to accurately capture shock propagation if the option for artificial explosion (thermal or kinetic bomb) is set in MESA. Among other advantages is the

ability of STELLA to provide reliable predictions for photometric properties of SN explosions without requiring large computational resources.

The paper is organised as follows: We describe the method and models in Section 2. In Section 3, we discuss our procedure of calibration of the thermalisation parameter in STELLA using representative models of SN Ia, SN Ipec, and SN IIP. We finalise the analysis in Section 4, where we specify the recommended value for the thermalisation parameter in STELLA.

## 2 INPUT MODELS AND METHOD

For the current study, we used three models from the literature. The goal is to explore the impact of different degrees of thermalisation of lines for application to:

- (i) normal SNe Ia — the basic W7 model ([Nomoto et al. 1984](#)).
- (ii) SNe Ipec — the 16-7b model from [Menon & Heger \(2017\)](#); [Menon et al. \(2019\)](#) exploded with the explosion energy of 2.33 foe (final kinetic energy 1.9 foe).
- (iii) normal SNe IIP — the L15 model from [Limongi et al. \(2000\)](#); [Utrobin et al. \(2017\)](#) exploded with the explosion energy of 1.1 foe (final kinetic energy 0.74 foe);

These three models are not universal for the three types of SNe we discuss, but serve as reference models for each type.

One of the main diagnostics for a possible ratio between scattering and absorptive line opacity is the inspection of spectra, specifically how lines redistribute energy within spectral bands. STELLA solves radiative transfer equations in a standard 100 frequency bins, which are not enough to construct detailed spectra. However, the code provides spectral energy distributions (hereafter, SED) which allow us to integrate flux in standard BESSEL broad bands. Therefore, the restriction on the thermalisation parameter might be determined through analysis of the broad band magnitudes. Below we analyse separately three SN types: SNe Ia, SNe Ipec, and SNe IIP.

The best way to calibrate the thermalisation parameter in STELLA is to compare to simulations calculated with advanced radiative transfer codes that do not use the simplified treatment of line opacity. These codes may allow photons to behave consistently with a set of calculated Non-LTE

<sup>1</sup> Modules for Experiments in Stellar Astrophysics <http://mesa.sourceforge.net/> ([Paxton et al. 2011, 2013, 2015, 2018](#)).

level populations, or at least without the requirement of a free parameter governing absorption and scattering. For SNe Type Ia we chose the widely-used W7 model to carry out comparison to the existing simulations done with the ARTIS code [Kromer & Sim \(2009\)](#). Compared to STELLA, ARTIS has the following advantages:

- (i) Each line is treated individually, without opacity binning.
- (ii) There is no concept of the thermalisation parameter. Radiation–matter interactions are always treated in detail (i.e. statistical equilibrium), e.g. the full macro-atom machinery is used to model fluorescence.
- (iii) Although it does not use Non-LTE level populations, ARTIS calculates a Non-LTE ionisation balance. It does this by recording detailed photoionisation rate estimators for the ground level of all ions, and approximating photoionisation rates of excited states by assuming that they scale with the ground level rates by the same factor as in LTE. Within an ionisation stage, the level populations are calculated from the Boltzmann distribution at the radiation temperature.

On top of that, we test our calibration based on comparison to observations, since ARTIS qualitatively reproduces realistic behaviour of the spectral energy distribution, i.e. broad band fluxes. For SNe IIP and SNe-IIpec, there are no well-accepted models. Therefore, we calibrate the STELLA thermalisation parameter via comparison to observations, assuming that sophisticated codes like CMFGEN, ARTIS, PHOENIX and others reproduce colours for observed normal SNe IIP and SN 1987A (i.e. SNe-IIpec) well.

### 3 DISCUSSION

#### 3.1 Application to SN Ia

We analyse the behaviour of the numerically computed STELLA light curves for comparison to simulations done with the radiative transfer code ARTIS, and observations of the normal SN Ia 2005cf ([Pastorello et al. 2007](#)). These light curves are shown in Figure 1.

The W7 model gives a reasonable match to the general colour evolution of SN2005cf, although there are significant discrepancies. Even though the W7 model is one choice of many candidate explosion models, and would therefore not be expected to match all of the features of SN 2005cf, we still use this combination of the theoretical model and observed data for our study. Note that we mapped into STELLA the hydrodynamical and chemical profiles of the model W7 which is exactly the same model used for ARTIS by [Kromer & Sim \(2009\)](#). Neither ARTIS nor STELLA simulations can explain the detailed behaviour of SN 2005cf, particularly, the second  $R$  and  $I$  maxima (see Figure 1). There are a number of reasons for this. The ARTIS curves clearly demonstrate the appearance of the second maximum which occurs a bit earlier than the observed maximum in SN 2005cf, and which is brighter ( $I$ ) than the observed one. It has been shown that non-LTE (either approximate or accurate) radiative transfer may better reproduce the second maxima ([Blondin et al. 2011, 2015](#)). Again, we emphasise that the model W7 itself is one particular choice of explosion model, and even

theoretically-perfect radiative transfer for this model will not necessarily match observed SNe Ia spectra. However, a number of explosion models can not reproduce the second maximum at all ([Ohlmann et al. 2014](#)). It could be that a slightly lower-mass model which host different thermodynamical conditions for the iron-group elements may better reproduce the maxima occurrence ([Blondin et al. 2017, 2018](#)). The yields of individual species like Sc, Ti, Cr, Fe, and radioactive  $^{56}\text{Ni}$ , and their distribution in the ejecta also strongly affect the location of the maxima ([Blondin et al. 2013; Shen et al. 2018](#)). As for STELLA, the code treats a limited number of species: H, He, C, N, O, Ne, Na, Mg, Al, Si, S, Ar, Ca, stable Fe, stable Ni, stable Co, radioactive  $^{56}\text{Ni}$ , and considers 150,000 lines in the standard settings ([Kurucz & Bell 1995](#)). Hence line lists for individual species like Sc, Ti, Cr are not included while they strongly contribute to line opacity. Hence, STELLA poorly reproduces the second maxima in general, although qualitatively represents colour evolution comparable with more sophisticated codes even with the limited number of lines ([Woosley et al. 2007](#)). Certainly, new physics and extensions to the line list in STELLA will be important areas of progress in future versions of the code.

In Figure 1, we present the results of our simulations of the model W7 done with STELLA and a range of values for the thermalisation parameter  $\epsilon$ . This allows us to explore the influence of different contributions to absorption and scattering in bound-bound transitions. We also superpose the results of the simulation by [Kromer & Sim \(2009\)](#) and the observed normal SN Ia 2005cf ([Pastorello et al. 2007](#)). We show six curves computed with STELLA with six corresponding thermalisation parameters: 100 % absorption (the label “Pure Absorption”), 90 % absorption + 10 % scattering (“90% Abs 10% Scat”), 80 % absorption + 20 % scattering (“80% Abs 20% Scat”), 50 % absorption + 50 % scattering (“50% Abs 50% Scat”), 10 % absorption + 90 % scattering (“10% Abs 90%Scat”), and 100 % scattering (“Pure Scattering”). Hence, we explore the variation of thermalisation parameter between 0 (pure scattering) and 1 (pure absorption). The general property of the STELLA light curves with different values for  $\epsilon$  is overestimated  $U$  magnitude, however presumably this is an intrinsic property of the given model. While  $U$  magnitude is almost independent on the choice of thermalisation parameter with moderate contribution of scattering ( $\epsilon = 0.8 - 1$ ), it has a stronger impact for  $R$  and  $I$  magnitudes.  $\epsilon = 0.5$  provides too broad light curve in  $B$ , therefore,  $\epsilon = 0.8 - 1$  is more realistic. Light curves calculated with larger contribution of scattering ( $\epsilon < 0.5$ ) are fully incompatible with the real observed data for SNe Ia. It is worth noting that light curves with  $\epsilon = 0.1$  have two pronounced maxima which are proven observational property of SNe Ia. We discuss this aspect below.

There are two major contributors to opacity in the W7 model – iron and calcium (considered by STELLA). As discussed in [Kasen \(2006\)](#), considering calcium lines as purely absorptive results in overestimated  $I$  magnitude. Therefore, SEDONA treats calcium lines as purely scattering, while iron lines tend to be purely absorptive. STELLA applies thermalisation parameter equally to all elements with no exceptions. With the currently implemented line list, STELLA does not resolve two maxima in  $I$  band. Surprisingly, the case with 90 % scattering does exhibit two maxima in the STELLA

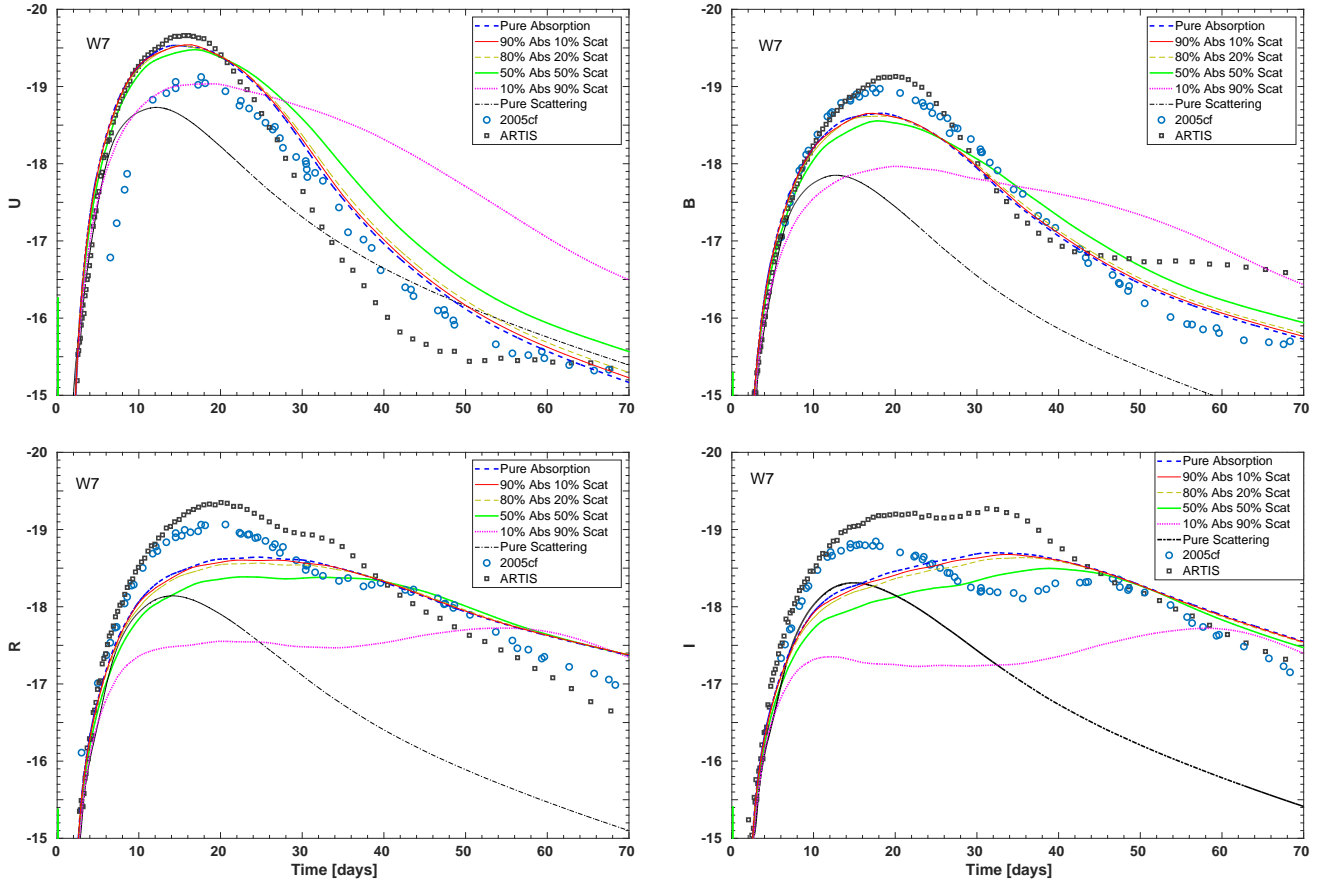


**Figure 1.** The broad-band magnitudes for the W7 model for different cases of the ratio between absorption and scattering computed with STELLA, broad-band magnitudes for the model W7 computed with ARTIS (Kromer & Sim 2009), and the observed magnitudes of SN 2005cf (Pastorello et al. 2007). “Abs” stands for absorption fraction, and “Scat” stands for scattering fraction. “Pure Absorption” means 100 % of absorption, and “Pure Scattering” means 100 % of scattering.

light curve, however both maxima are underestimated in luminosity. This means that at least some strong lines, i.e. most likely calcium lines, have to be treated with sufficiently low thermalisation parameter, e.g.  $\varepsilon = 0.1$ , i.e. almost purely scattering. As a consequence,  $U$  band light curve for the case of  $\varepsilon = 0.1$  is much closer to the observed magnitude of SN 2005cf. Nevertheless, the widths of the light curves in all bands are too large and inconsistent with the observed data.

In Figure 2, we show STELLA SEDs for the model W7 for different values of thermalisation parameter at day 15 and day 40. SED maxima for the cases with 100 %, 90 %, 80 %, and 50 % absorption are very close to each other at day 15, although the exact maximum wavelength differs by 300 Å. At a later epoch, day 40, the cases of 100 %, 90 %, and 80 % are almost identical, while the case of 50 % provides relatively bluer spectrum. Therefore, we rule out values for thermalisation parameter below 0.8. If comparing our SEDs to the result of spectral synthesis simulations by SEDONA (Fig. 5, Kasen et al. 2006) and ARTIS (Fig. 6, Kromer & Sim 2009), we conclude that spectral maximum lies around 3500 Å and around 6000–6500 Å at day 15 and day 40, respectively, i.e. thermalisation parameter tends to be close to unity.

We carry out a quantitative analysis, particularly, we calculated the linear Pearson’s correlation coefficient with the 95 % confidence interval to pick the most plausible value for

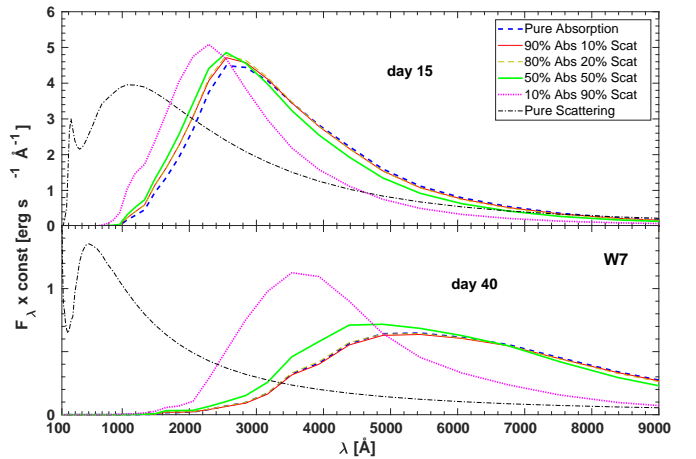


**Figure 2.** Spectral energy distribution for the model W7 with different values of thermalisation parameter: 1 (blue dashed), 0.9 (red), 0.8 (yellow dashed), 0.5 (green), 0.1 (magenta dotted), and 0 (black dash-dotted), at day 15 and day 40. Labels have the same meaning as in Figure 1.

the thermalisation parameter (e.g., for the correlation between 2005cf and the STELLA curves). We have confirmed that our findings with the correlation method are in agree-



ment with several alternative statistical methods to quantify the best-fit (for details, see Appendix A). The observed data and the synthetic light curves are sampled on different grids of time points. Therefore, we first applied a 10-th order polynomial regression or smoothing spline (using Matlab standard libraries) with the least standard deviation criterion. We then evaluated the resulting polynomial (or spline) on 100 equidistant time points. We therefore converted each light curve into a vector of a uniform length, discretised onto a regular time grid. The  $\chi$ -squared test evaluates statistical dependence between standard deviations under the condition of normally distributed residuals.  $\chi$ -squared test was not considered because (1) given arrays are very limited in time, (2) the data points within a given array are not independent, and (3) residuals do not have normal distribution. Therefore, we choose the estimate of the correlation coefficient in the linear regression approach as a measure of statistical coherence between vectors. This method was applied to every curve in the study. Correlation analysis, i.e. evaluation of statistical dependence, was based on the calculation of the Pearson's correlation coefficient in the frame of the linear regression model (Afifi & Azen 1979; Aivazyan et al. 1985):

$$r = \frac{\sum_{i=1}^N (x_i - \langle x \rangle)(y_i - \langle y \rangle)}{\sqrt{\sigma_x \sigma_y}}, \quad (1)$$

where  $\langle x \rangle$  and  $\langle y \rangle$  are the means, and  $\sigma_x$  and  $\sigma_y$  are the standard deviation for light curve vectors  $x$  and  $y$ , respectively. The correlation analysis was carried out for each pair of curves: U-band 2005cf and U-band STELLA curve, B-band 2005cf and B-band STELLA curve and so on. The interval is chosen between day 2 and day 85 for STELLA-2005cf correlation. The same method was applied for pairs of ARTIS and STELLA curves. The interval is 2-72 days for ARTIS-STELLA correlation. In each pair of curves, the interval is chosen to be the longest time interval over which both curves are defined.

We analyse correlation between STELLA and ARTIS, and STELLA and SN 2005cf. The closest correlation between STELLA and ARTIS is observed for the cases of 100%, 90%, and 80% of absorption with the coefficients 0.975, 0.953, 0.980, 0.899–0.919, and 0.899–0.918 for  $U$ ,  $B$ ,  $V$ ,  $R$ , and  $I$ , correspondingly. Since we look for the choice which includes at least some scattering, we conclude that the best cases are 80% and 90% absorption. We apply the same procedure to correlate STELLA and SN 2005cf. The resulting correlation coefficients show the tight correlation for the cases of thermalisation parameter  $\varepsilon = 0.5$  for  $U$  band with coefficient 0.987, and for  $\varepsilon = 0.8 - 1$  with coefficient 0.995, 0.999, 0.894–0.909, and 0.862–0.878 for  $B$ ,  $V$ ,  $R$ , and  $I$ , respectively. To conclude, we suggest to set thermalisation parameter between 0.8 and 0.9, and more precisely  $\varepsilon = 0.9$  for consistency with SNeII which we discuss in the sections below.

We conclude that correlation coefficients derived for STELLA–SN 2005cf are the same as for STELLA–ARTIS. Therefore, we follow the same procedure for SNe type IIP and 87A-like, namely we analyse the correlation between the STELLA light curves and observed data to define the plausible thermalisation parameter. On top of that, calibrating the code parameter on the real observations complements our anal-

ysis, and makes future numerical simulations with STELLA even more robust.

### 3.2 Application to SN 1987A

Modelling of the progenitor of SN 1987A is still an open question, and there is no model that accurately reproduces all observed features. There are single star models (Woosley 1988; Shigeyama & Nomoto 1990), and binary models (Menon & Heger 2017; Urushibata et al. 2018; Ono et al. 2020). Among the difficulties is the problem of producing a blue supergiant model at LMC metallicity. Single star models are computed with artificially reduced metal content to get a relatively compact ( $\sim 50 R_{\odot}$ ) progenitor. Models with the low metal content, i.e. low metallicity, provide too blue colours, particularly,  $U$  band magnitude is overestimated (Blinnikov 1999). At the same time, binary merger models by Menon & Heger (2017) have sufficient metals because of accretion from the companion, and they are more promising as an explanation for, particularly, the  $U$  magnitude of SN 1987A. Therefore, we pick up one of their recent binary models, 16-7b (Menon et al. 2019), to calibrate the thermalisation parameter in STELLA.

The light curves taken with different values of thermalisation parameter are shown in Figure 3. Figure 3 shows bolometric light curves (upper left) which are in acceptable agreement with observations for the chosen exposition energy of 2.33 foe.  $U$  and  $B$  magnitudes are the most affected by variation in the thermalisation parameter, while variation in  $V$ ,  $R$ , and  $I$  magnitudes is not large for different parameter values. We show  $U$ ,  $B$  and  $I$  magnitudes for demonstration. We note that we do not pay attention to the radioactive tail, but mostly concentrate on the photospheric phase, i.e. before approximately day 120. STELLA does not provide reliable broad-band magnitudes after this epoch, since the SN ejecta becomes semi-transparent, and Non-LTE treatment is required. For quantitative analysis, we apply the same correlation procedure as discussed in Section 3.1. Hence we calculate the correlation coefficients between the numerical STELLA light curves in broad bands and broad band magnitudes of SN 1987A (Menzies et al. 1987). Light curves computed with  $\varepsilon = 0.8, 0.9$  and 1 evolve close to each other. However, taking into account the necessity of a contribution from resonant scattering, we conclude that  $\varepsilon$  has to be lower than 1, e.g. 0.8–0.9. From the correlation analysis, the most suitable value for the thermalisation parameter lies between 0.8 and 1, if we ignore the a priori irrelevant values corresponding to pure scattering and the case with 10% of absorption. The correlation coefficients are: 0.911–0.926, 0.872–0.899, 0.9–0.917, 0.936, and 0.947, for  $U$ ,  $B$ ,  $V$ ,  $R$ , and  $I$ , respectively.

Additionally, we did a test using the spectral synthesis code ARTIS for the model B15-2 (Utrobín et al. 2015) which is similar to the model 16-7b in our study except for a zero metallicity. We run the model with a low number of photon packets to explore the contribution by resonance scattering and true absorption. The photon packets experience 252130, 265155, 162141, and 3152 line interactions in timesteps at day 60, day 80, day 100, and day 140, while 4943, 5324, 3984, and 159 of those are pure scattering (i.e. no wavelength change). Hence, the thermalisation parameter, i.e. the ratio between the number of inelastic interactions

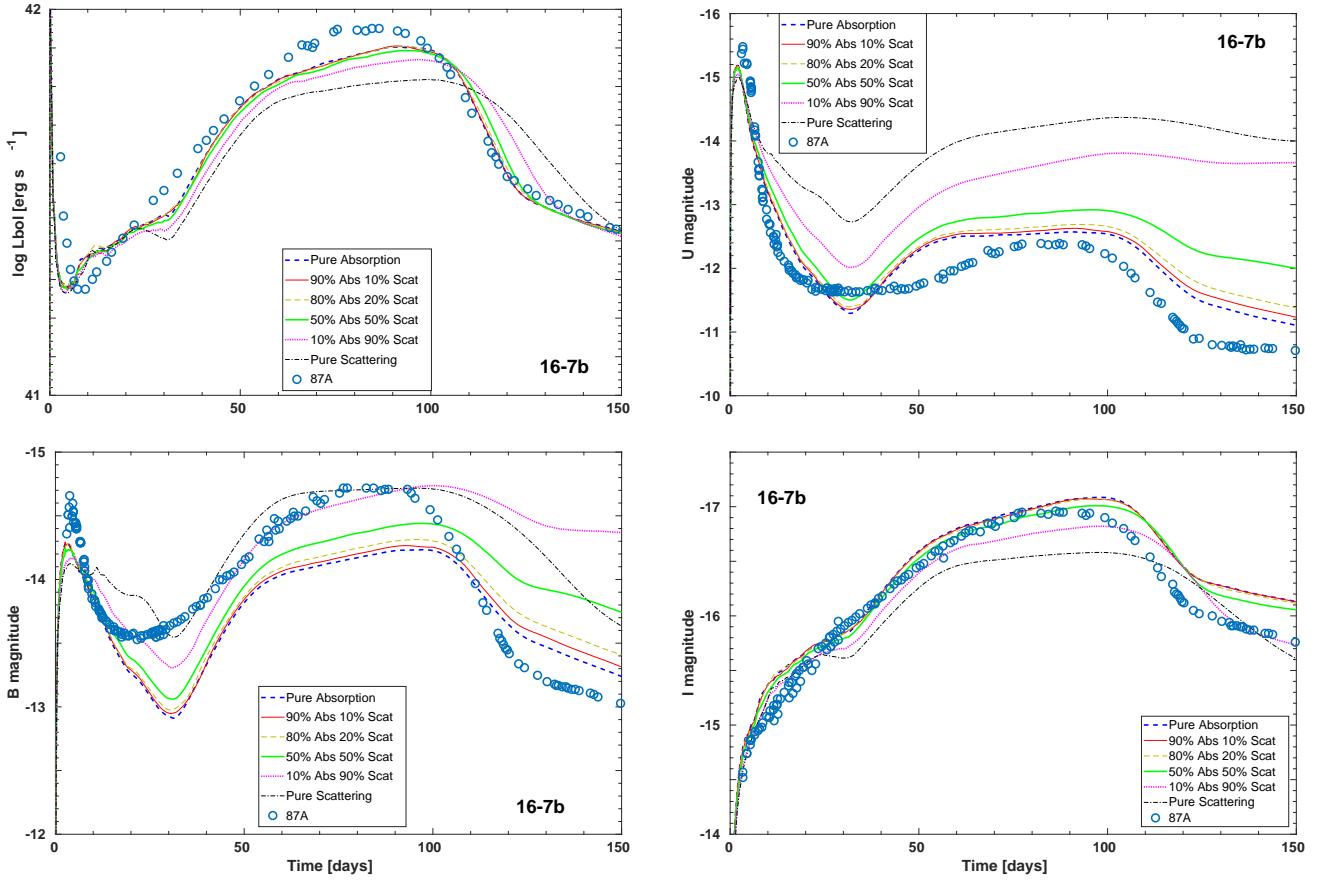


**Figure 3.** Bolometric light curves and  $U$ ,  $B$  and  $I$  broad-band magnitudes for the model 16-7b for different cases of the ratio between absorption and scattering. Labels have the same meaning as in Figure 1.

(absorption) and total number of interactions is: 0.98, 0.98, 0.975, and 0.95 for corresponding epochs. These numbers are very close to unity, i.e. they show the dominant contribution of absorption to the line opacity. However, this also demonstrates the inevitability of a non-zero scattering fraction in the line opacity.

From our analysis, we conclude that the thermalisation parameter for hydrogen-rich SNe like SN 1987A falls into the same interval as for Ni-powered SNe Ia, i.e. 0.8–0.9, with the highest plausible value of 0.9.

### 3.3 Application to SNe IIP

The model L15 is the accepted model which reproduces bolometric properties of SN 1999em (Elmhamdi et al. 2003; Utrobin 2007; Utrobin et al. 2017). In Figure 4, we show bolometric light curves and broad-band magnitudes for the model L15 for different cases of the ratio between absorption and scattering. Firstly, we present bolometric light curves for the subset of the model L15 (the upper left plot in Figure 4) to demonstrate that the model is indeed sufficient to explain the bolometric luminosity of SN 1999em. As in previous sections, we vary the thermalisation parameter between 0 and 1 for the model L15. The overall differences between bolometric light curves are not large. There is a tiny variation in early plateau luminosity (maximum 0.05 dex), while there is a noticeable difference in the behaviour of the transition

of the light curve to the radioactive tail. Nevertheless, the treatment of lines is indeed not important for the bolometric properties at earlier epoch because lines contribute less significantly than the continuum opacity during the early phase and especially during the relaxation after shock breakout. However, the lines start playing a significant role at day 20 for our model L15 (see Figure 4). In any case, the bolometric light curve is rather insensitive to different degrees of thermalisation in lines because it reflects the overall energy budget (which is conserved), while different thermalisation values only cause redistribution of energy between parts of the spectrum.

With the pure scattering line opacity,  $U$  and  $B$  remain blue for the entire plateau. Blue photons from the decay of  $^{56}\text{Ni}$  are accumulated in the region where they are born. Line opacity is much higher for blue photons than for redder photons, with the effect that blue photons require a longer time to diffuse through the optically-thick medium. Therefore, scattering-dominated line opacity provides a larger fraction of blue photons remaining in the inner region of the SN ejecta. Assuming SN 1999em to be a normal SN IIP,  $U$  fades during the plateau phase with the slope 4–5 mags during 100 days, and  $B$  magnitude drops with the slope 2 mags during this period. This is consistent with our modelled curves with scattering fraction of 0–20%. Observations by Faran et al. (2014), Valenti et al. (2016) and Szalai et al. (2019) also confirm these slopes and present a large set of

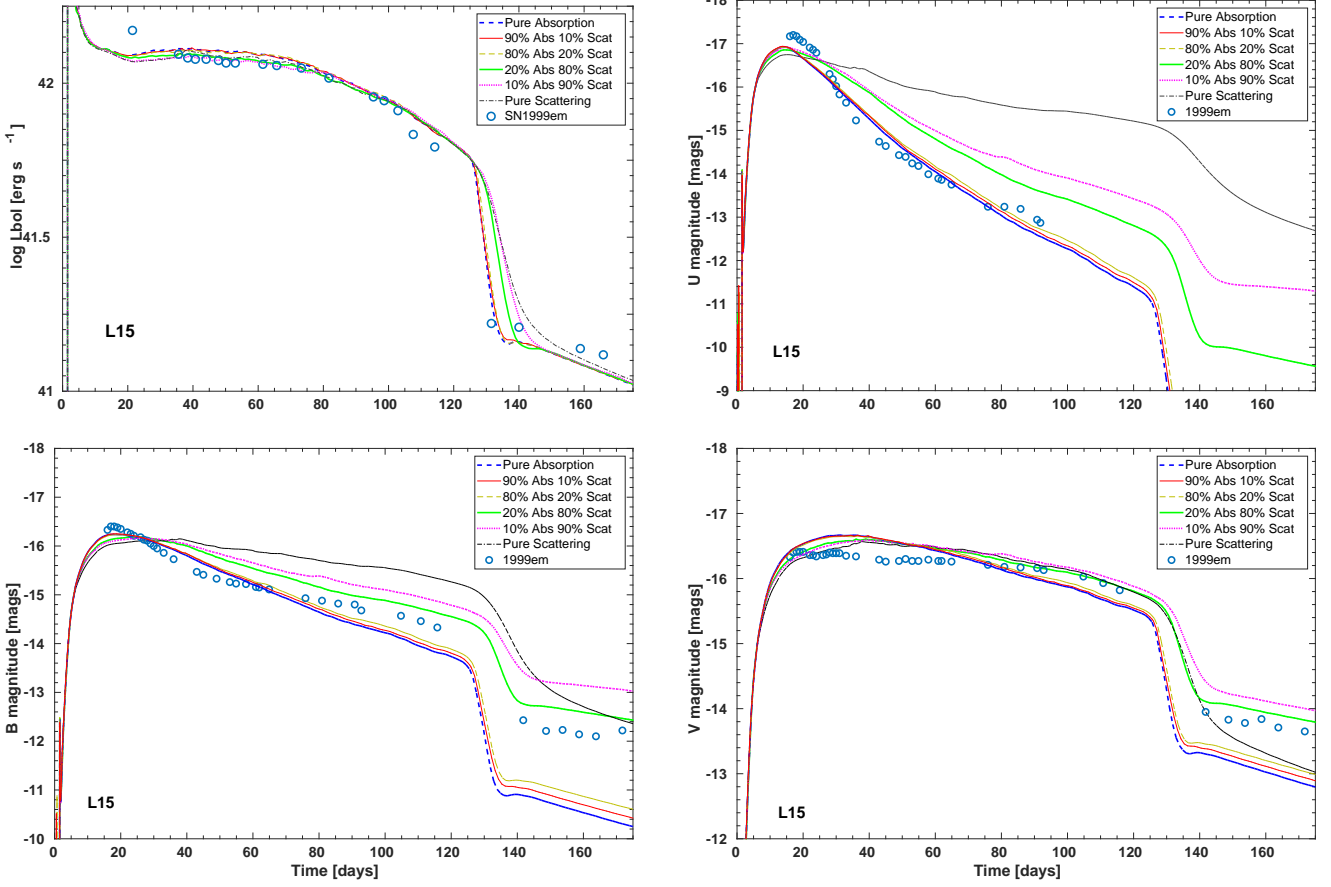


**Figure 4.** Bolometric light curves and broad-band magnitudes for the model L15 for different cases of the ratio between absorption and scattering. We superpose observed SN 1999em as crosses (Elmhamdi et al. 2003). Labels have the same meaning as in Figure 1 except the magenta curve, which stands now for the case of 20 % of absorption and 80 % of scattering.

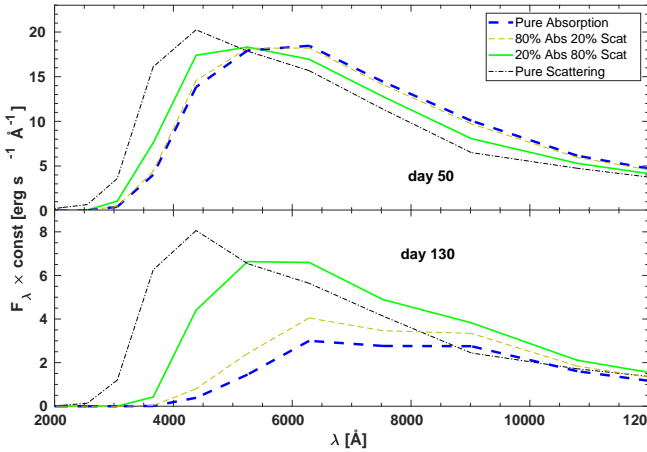


**Figure 5.** Spectral energy distribution for the model L15 for cases of 0 % (blue dashed), 20 % (red), 80 % (green dashed), and 100 % (magenta) of scattering at day 50 and day 130. Labels have the same meaning as in Figure 4.

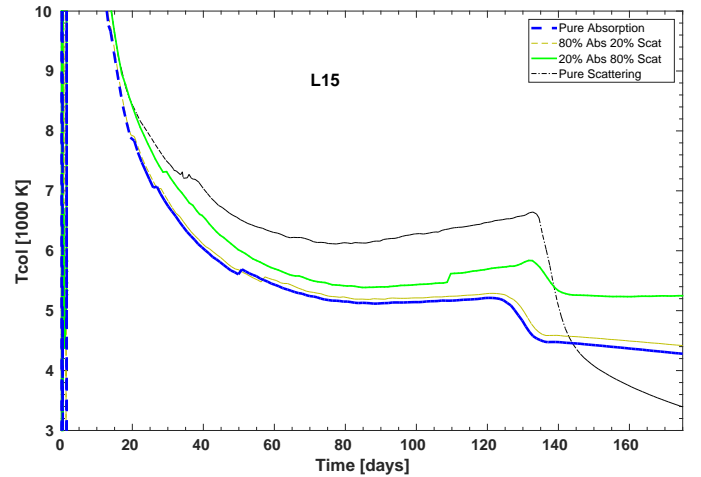


**Figure 6.** Colour temperature evolution for the model L15 for cases of 0 % (blue dashed), 20 % (red), 80 % (green dashed), and 100 % (magenta) of scattering. Labels have the same meaning as in Figure 4.

SNe IIP which show standard decline of about 2 mags in *B* band during 100 days. *R* and *I* light curves are not strongly affected by the value of the thermalisation parameter. We conclude that introducing a larger fraction of scattering to

the line opacity leads to long-lasting blue colours which is not supported by observations of normal SNe IIP.

We follow the same correlation procedure as we applied

for SNe Ia and SNe 1987A-like. We found that the light curves with  $\varepsilon = 0.8, 0.9,$  and  $1$  are the most correlated with the observed broad-band magnitudes of SN 1999em. The correlation coefficients are:  $0.98, 0.992,$  and  $0.992$  for  $U, B,$  and  $V,$  respectively.

In Figure 5, we show spectral energy distributions for the model L15 for cases of 0 %, 20 %, 80 %, and 100 % of scattering at day 50 and day 130. There is an extra blue flux for those cases where scattering fraction is higher, which leads to higher colour temperature. Figure 6 shows corresponding colour temperature evolution for these cases. While pure absorption (what means 0 % scattering) and 20 % scattering cases are suitable for normal SNe IIP (see e.g., Bersten & Hamuy 2009), curves with larger scattering contribution are totally unrealistic, because of relatively too-blue colour at the end of their plateau.

To conclude, we find the value  $\varepsilon = 0.9$  provides the best match to colours in normal SNIIP.

#### 4 CONCLUSIONS

We explored the treatment of lines in the hydrodynamics radiative transfer code STELLA. Previously, all lines in the code were considered as purely absorptive, i.e. a photon was immediately thermalised on interaction with matter. We analysed the impact of introduction scattering into the line treatment using three reference models, W7 (Nomoto et al. 1984), 16-7b (Menon & Heger 2017; Menon et al. 2019), and L15 (Limongi et al. 2000; Utrobin et al. 2017), to illustrate the impact of different degree of thermalisation in lines on the behaviour of light curves and SEDs of normal SNe Ia, SNe Ipec, and normal SNe IIP. We analysed light curves in the broad bands in the context of the more sophisticated simulations done with the code ARTIS, and well-observed SN 2005cf, SN 1987A, and SN 1999em.

We found that the most suitable value for the thermalisation parameter  $\varepsilon$ , i.e. the relative contribution of absorption to overall line opacity, lies between 0.8 and 0.9 for the three types of SNe considered. The scattering due to lines should be less than 10–20 % to prevent blue flux from exceeding observed SNe.

Our recommendation is to use  $\varepsilon = 0.9$  in all future simulations that will be done with the code STELLA which is a part of the latest MESA release (Paxton et al. 2018).

#### ACKNOWLEDGMENTS

We thank the referee Prof. Saurabh W. Jha for his interest in our study and careful analysis of our methodology and results that improved the paper. AK is supported by the Alexander von Humboldt Foundation. LS acknowledges support from STFC through grant, ST/P000312/1. SB and PB are sponsored by grant RSF 18-12-00522. Some of this work was performed using the Cambridge Service for Data Driven Discovery (CSD3), part of which is operated by the University of Cambridge Research Computing on behalf of the STFC DiRAC HPC Facility (www.dirac.ac.uk). The DiRAC component of CSD3 was funded by BEIS capital funding via STFC capital grants ST/P002307/1 and ST/R002452/1 and STFC operations grant ST/R00689X/1. DiRAC is part

of the National e-Infrastructure. The authors thank Viktor Utrobin, Thomas Janka for discussions which initiated this study, and Markus Kromer and Stuart Sim for clarifications about ARTIS simulations, Anders Jerkstrand, Ildar Khabibullin and Marat Potashov for overall discussions.

#### DATA AVAILABILITY

The data computed and analysed for the current study are available via link <https://www.mpa-garching.mpg.de/ccsnarchive/data/Kozyreva2018/index.html>.

#### REFERENCES

- Affi A., Azen S. P., 1979, *Statistical Analysis. A Computer Oriented Approach*. Academic Press, New York - San Francisco - London. 488 pp.
- Aivazyan S., Yenyukov I. S., Meshalkin L., 1985, *Applied Statistics. Study of Relationships*. Moscow, Finansy i statistika. 487 pp.
- Baron E., Hauschildt P. H., Mezzacappa A., 1996a, *MNRAS*, **278**, 763
- Baron E., Hauschildt P. H., Nugent P., Branch D., 1996b, *MNRAS*, **283**, 297
- Bersten M. C., Hamuy M., 2009, *ApJ*, **701**, 200
- Bersten M. C., Benvenuto O., Hamuy M., 2011, *ApJ*, **729**, 61
- Blinnikov S. I., 1999, *Astronomy Letters*, **25**, 359
- Blinnikov S. I., Eastman R., Bartunov O. S., Popolitov V. A., Woosley S. E., 1998, *ApJ*, **496**, 454
- Blondin S., Kasen D., Röpke F. K., Kirshner R. P., Mandel K. S., 2011, *MNRAS*, **417**, 1280
- Blondin S., Dessart L., Hillier D. J., Khokhlov A. M., 2013, *MNRAS*, **429**, 2127
- Blondin S., Dessart L., Hillier D. J., 2015, *MNRAS*, **448**, 2766
- Blondin S., Dessart L., Hillier D. J., Khokhlov A. M., 2017, *MNRAS*, **470**, 157
- Blondin S., Dessart L., Hillier D. J., 2018, *MNRAS*, **474**, 3931
- Dessart L., Hillier D. J., 2010, *MNRAS*, **405**, 2141
- Eastman R. G., Pinto P. A., 1993, *ApJ*, **412**, 731
- Elmhamdi A., et al., 2003, *MNRAS*, **338**, 939
- Faran T., et al., 2014, *MNRAS*, **442**, 844
- Goldstein D. A., Kasen D., 2018, *ApJ*, **852**, L33
- Höflich P., 1995, *ApJ*, **443**, 89
- Jerkstrand A., Fransson C., Kozma C., 2011, *A&A*, **530**, A45
- Kasen D., 2006, *ApJ*, **649**, 939
- Kasen D., Thomas R. C., Nugent P., 2006, *ApJ*, **651**, 366
- Kromer M., Sim S. A., 2009, *MNRAS*, **398**, 1809
- Kurucz R. L., Bell B., 1995, *Atomic line list*
- Limongi M., Straniero O., Chieffi A., 2000, *ApJS*, **129**, 625
- Lucy L. B., 1999, *A&A*, **345**, 211
- Magee M. R., Sim S. A., Kotak R., Kerzendorf W. E., 2018, *A&A*, **614**, A115
- Mazzali P. A., Lucy L. B., 1993, *A&A*, **279**, 447
- Menon A., Heger A., 2017, *MNRAS*, **469**, 4649
- Menon A., Utrobin V., Heger A., 2019, *MNRAS*, **482**, 438
- Menzies J. W., et al., 1987, *MNRAS*, **227**, 39P
- Nomoto K., Thielemann F.-K., Yokoi K., 1984, *ApJ*, **286**, 644
- Nugent P., Baron E., Branch D., Fisher A., Hauschildt P. H., 1997, *ApJ*, **485**, 812
- Ohlmann S. T., Kromer M., Fink M., Pakmor R., Seitenzahl I. R., Sim S. A., Röpke F. K., 2014, *A&A*, **572**, A57
- Ono M., Nagataki S., Ferrand G., Takahashi K., Umeda H., Yoshida T., Orlandi S., Miceli M., 2020, *ApJ*, **888**, 111
- Pastorello A., et al., 2007, *MNRAS*, **376**, 1301



- Paxton B., Bildsten L., Dotter A., Herwig F., Lesaffre P., Timmes F., 2011, *ApJS*, **192**, 3
- Paxton B., et al., 2013, *ApJS*, **208**, 4
- Paxton B., et al., 2015, *ApJS*, **220**, 15
- Paxton B., et al., 2018, *ApJS*, **234**, 34
- Pinto P. A., Eastman R. G., 2000, *ApJ*, **530**, 757
- Piro A. L., Morozova V. S., 2014, *ApJ*, **792**, L11
- Shen K. J., Kasen D., Miles B. J., Townsley D. M., 2018, *ApJ*, **854**, 52
- Shigeyama T., Nomoto K., 1990, *ApJ*, **360**, 242
- Szalai T., et al., 2019, arXiv e-prints,
- Urushibata T., Takahashi K., Umeda H., Yoshida T., 2018, *MNRAS*, **473**, L101
- Utrobin V. P., 2007, *A&A*, **461**, 233
- Utrobin V. P., Wongwathanarat A., Janka H.-T., Müller E., 2015, *A&A*, **581**, A40
- Utrobin V. P., Wongwathanarat A., Janka H.-T., Müller E., 2017, *ApJ*, **846**, 37
- Valenti S., et al., 2016, *MNRAS*, **459**, 3939
- Wollaeger R. T., van Rossum D. R., Graziani C., Couch S. M., Jordan IV G. C., Lamb D. Q., Moses G. A., 2013, *ApJS*, **209**, 36
- Woosley S. E., 1988, *ApJ*, **330**, 218
- Woosley S. E., Kasen D., Blinnikov S., Sorokina E., 2007, *ApJ*, **662**, 487

value for the thermalisation parameter. We list the coefficients for the combination ARTIS–STELLA in the  $U$ ,  $V$ ,  $R$ , and  $I$  broad bands in Table A2.

In Figures A2, A3, and A4, we demonstrate the  $B$ -band STELLA magnitudes and corresponding magnitudes of the SN 2005cf, SN 1987A, and SN 1999em. Tables A3, A4, and A5 contain calculated coefficients for the cases considered in the paper: the model W7 and SN 2005cf, the model 16-7b and SN 1987A, and the model L15 and SN 1999em.

This paper has been typeset from a  $\text{\TeX}/\text{\LaTeX}$  file prepared by the author.

## APPENDIX A: ADDITIONAL STATISTICS

We carried out additional statistical tests to verify the results of the correlation method that we used in Section 3.

Let us consider the pairs of arrays from our study, namely, the  $B$ -band magnitudes calculated with ARTIS and STELLA (with different degree of thermalisation). In Figure A1, we demonstrate the pairs of arrays: ARTIS  $B$ -band magnitude versus STELLA  $B$ -band magnitude computed with different value of the thermalisation parameter. We calculated the linear regression coefficient for each pair, assuming  $Y = A \times X + B$ , where  $X$  is ARTIS magnitude and  $Y$  is STELLA magnitude.

We consider the statistic:

$$s = \sum_i [(y_i - \langle y \rangle) - (x_i - \langle x \rangle)]^2 \quad (\text{A1})$$

and slightly modified statistic:

$$s_m = \sum_i \left[ \frac{y_i - \langle y \rangle}{\langle y \rangle} - \frac{x_i - \langle x \rangle}{\langle x \rangle} \right]^2. \quad (\text{A2})$$

The minimal value for these statistics will indicate the best match between arrays  $X$  and  $Y$ .

In Table A1, we list the resulting coefficients. Here,  $A$  is linear regression coefficient,  $r$  is linear correlation coefficient (see Equation 1 in Section 3.1), and two coefficients  $s$  and  $s_m$  counting for the proposed additional statistics. The maximal correlation coefficient correspond to minimal  $s$  and  $s_m$  coefficients. We note though that maximal  $r$  and minimal  $s/s_m$  do not necessarily correspond to the maximal linear regression coefficient (its closure to 1). We highlight in bold face the best match according to all considered statistics. Hence, we rely on the maximal correlation coefficient in the main body of the paper as the diagnostic for the best match between light curves and the selection of the best

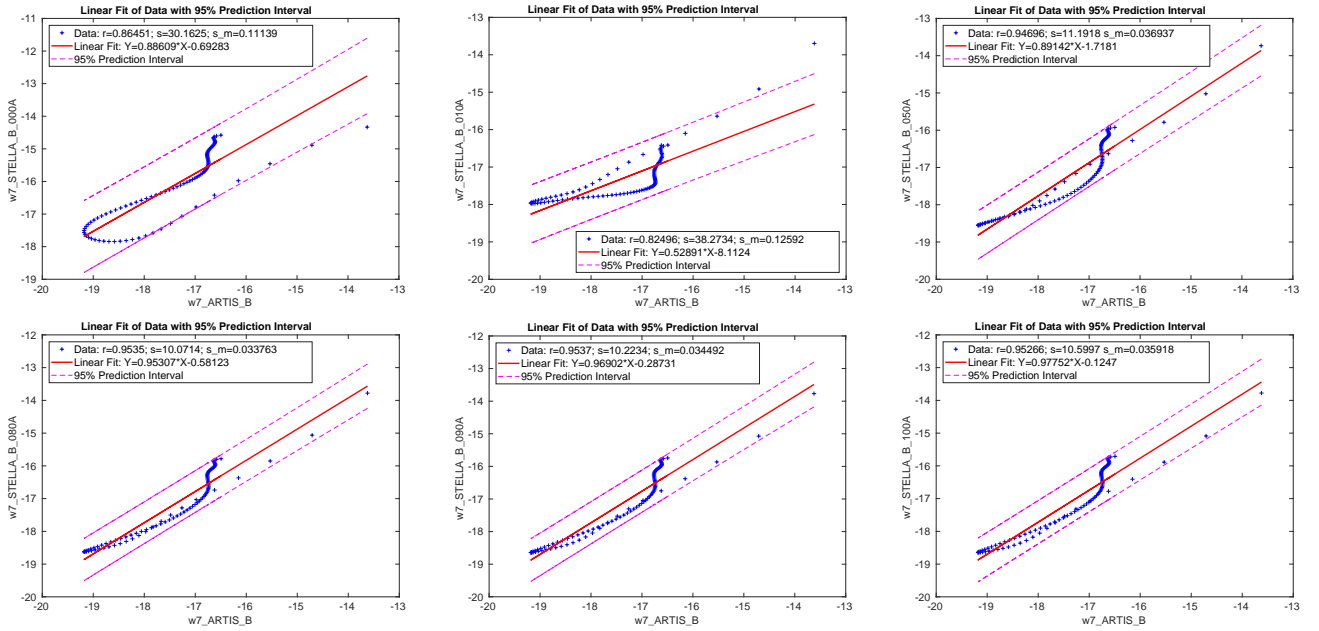


**Figure A1.** The  $B$ -band magnitudes of the W7 model computed with STELLA using different assumed ratios between absorption and scattering, and the W7 model computed with ARTIS (Kromer & Sim 2009).

**Table A1.** The linear regression coefficient  $A$ , linear correlation coefficient  $r$ , and the statistics  $s$  and  $s_m$  for the pairs of light curves in  $B$  broad band computed with STELLA and ARTIS. The line in bold face corresponds to the maximum correlation coefficient and minimum  $s$  and  $s_m$  coefficients.

		$A$	$r$	$s$	$s_m$
BARTIS	B_STELLA_000A	0.88609	0.86451	30.1625	0.11139
BARTIS	B_STELLA_010A	0.52891	0.82496	38.2734	0.12592
BARTIS	B_STELLA_050A	0.89142	0.94696	11.1918	0.036937
BARTIS	B_STELLA_080A	0.95307	0.95350	10.0714	0.033763
<b>BARTIS</b>	<b>B_STELLA_090A</b>	<b>0.96902</b>	<b>0.95370</b>	<b>10.2234</b>	<b>0.034492</b>
BARTIS	B_STELLA_100A	0.97752	0.95266	10.5997	0.035918

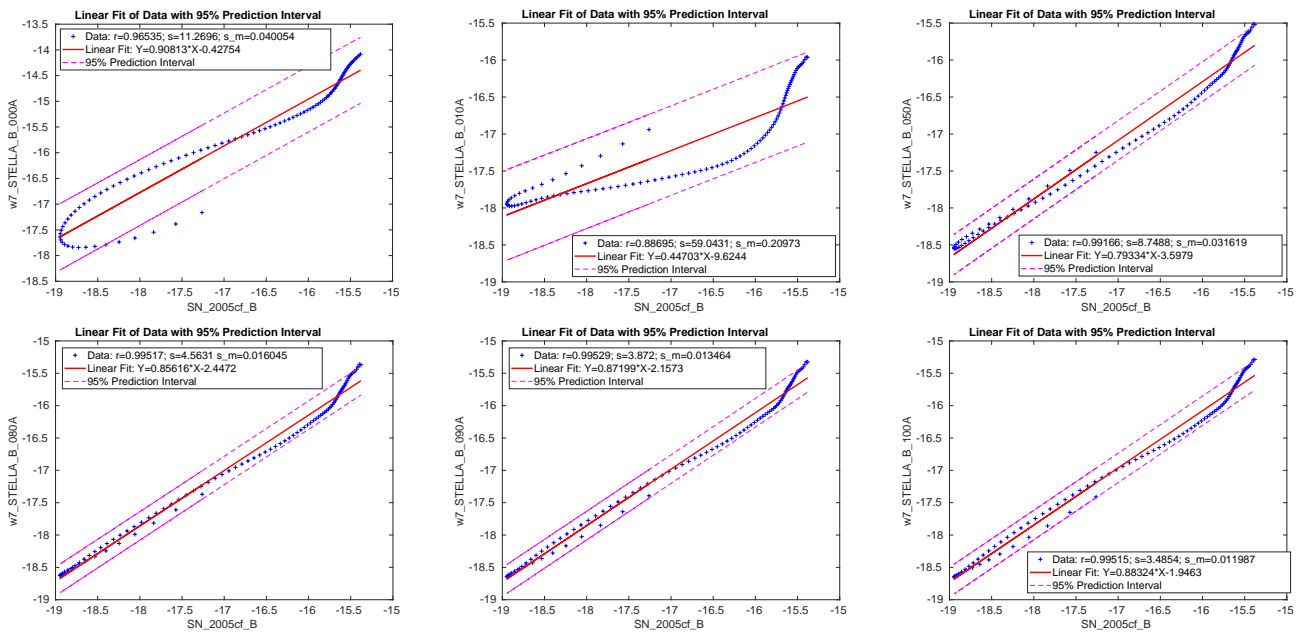


**Figure A2.** The  $B$ -band magnitudes of the W7 model computed with STELLA using different assumed ratios between absorption and scattering, and observations of SN 2005cf.

**Table A2.** The same as in Table A1 for the W7 U,V,R,I-band STELLA magnitudes and ARTIS magnitudes.

		$A$	$r$	$s$	$s_m$
U_ARTIS	U_STELLA_000A	0.64213	0.97445	40.67760	0.13968
U_ARTIS	U_STELLA_010A	0.44048	0.80076	114.35609	0.41186
U_ARTIS	U_STELLA_050A	0.81061	0.95934	25.15613	0.09365
U_ARTIS	U_STELLA_080A	0.88321	0.97406	15.11910	0.05550
U_ARTIS	U_STELLA_090A	0.90048	0.97608	13.59926	0.04947
U_ARTIS	U_STELLA_100A	0.91200	0.97707	12.81158	0.04621
V_ARTIS	V_STELLA_000A	0.88609	0.86451	30.1625	0.11139
V_ARTIS	V_STELLA_010A	0.52891	0.82496	38.2734	0.12592
V_ARTIS	V_STELLA_050A	0.89142	0.94696	11.1918	0.036937
V_ARTIS	V_STELLA_080A	0.95307	0.95350	10.0714	0.033763
V_ARTIS	V_STELLA_090A	0.96902	0.95370	10.2234	0.034492
V_ARTIS	V_STELLA_100A	0.97752	0.95266	10.5997	0.035918
R_ARTIS	R_STELLA_100A	0.84774	0.86779	27.72292	0.09397
R_ARTIS	R_STELLA_100A	0.25819	0.51068	79.17357	0.24369
R_ARTIS	R_STELLA_100A	0.55486	0.84413	34.52384	0.10564
R_ARTIS	R_STELLA_100A	0.61134	0.89904	25.67382	0.07864
R_ARTIS	R_STELLA_100A	0.62611	0.91026	23.65941	0.07251
R_ARTIS	R_STELLA_100A	0.63532	0.91865	22.23886	0.06819
I_ARTIS	I_STELLA_100A	0.84681	0.78094	39.04812	0.13263
I_ARTIS	I_STELLA_100A	0.26291	0.47073	63.65931	0.19110
I_ARTIS	I_STELLA_100A	0.63093	0.84502	23.93898	0.07053
I_ARTIS	I_STELLA_100A	0.69274	0.89938	16.82663	0.04937
I_ARTIS	I_STELLA_100A	0.70765	0.91048	15.28726	0.04483
I_ARTIS	I_STELLA_100A	0.71676	0.91804	14.25680	0.04180

**Table A3.** The same as Table A1 for the W7 STELLA broad-band magnitudes and SN 2005cf magnitudes.

		$A$	$r$	$s$	$s_m$
U_sn2005cf	U_STELLA_000A	0.81004	0.96627	17.38413	0.06189
U_sn2005cf	U_STELLA_010A	0.67581	0.93254	36.48919	0.14668
U_sn2005cf	U_STELLA_050A	1.05999	0.99128	4.92997	0.01490
U_sn2005cf	U_STELLA_080A	1.13471	0.99130	8.58731	0.02674
U_sn2005cf	U_STELLA_090A	1.15321	0.99087	10.11125	0.03232
U_sn2005cf	U_STELLA_100A	1.16688	0.99045	11.40321	0.03729
B_sn2005cf	B_STELLA_000A	0.90813	0.96535	11.26962	0.04005
B_sn2005cf	B_STELLA_010A	0.44703	0.88695	59.04310	0.20973
B_sn2005cf	B_STELLA_050A	0.79334	0.99166	8.74879	0.03162
B_sn2005cf	B_STELLA_080A	0.85616	0.99517	4.56309	0.01604
B_sn2005cf	B_STELLA_090A	0.87199	0.99529	3.87200	0.01346
B_sn2005cf	B_STELLA_100A	0.88324	0.99515	3.48541	0.01199
V_sn2005cf	V_STELLA_000A	1.22312	0.93853	20.54001	0.09563
V_sn2005cf	V_STELLA_010A	0.30969	0.82297	42.53423	0.13506
V_sn2005cf	V_STELLA_050A	0.65986	0.99167	10.02148	0.03177
V_sn2005cf	V_STELLA_080A	0.72819	0.99885	6.11644	0.01934
V_sn2005cf	V_STELLA_090A	0.74629	0.99915	5.31970	0.01679
V_sn2005cf	V_STELLA_100A	0.76039	0.99922	4.75023	0.01496
R_sn2005cf	R_STELLA_000A	1.24223	0.91316	25.27996	0.10852
R_sn2005cf	R_STELLA_010A	0.24682	0.55332	48.70329	0.15306
R_sn2005cf	R_STELLA_050A	0.60890	0.88714	17.48942	0.05509
R_sn2005cf	R_STELLA_080A	0.67632	0.92815	12.31342	0.03897
R_sn2005cf	R_STELLA_090A	0.69377	0.93631	11.15055	0.03535
R_sn2005cf	R_STELLA_100A	0.70649	0.94276	10.26031	0.03257
I_sn2005cf	I_STELLA_000A	1.45465	0.90383	32.08675	0.12960
I_sn2005cf	I_STELLA_010A	0.09844	0.28903	43.30838	0.13566
I_sn2005cf	I_STELLA_050A	0.54445	0.82089	16.53865	0.05180
I_sn2005cf	I_STELLA_080A	0.61584	0.86225	13.11988	0.04129
I_sn2005cf	I_STELLA_090A	0.63418	0.87236	12.25684	0.03864
I_sn2005cf	I_STELLA_100A	0.64790	0.87824	11.70627	0.03694

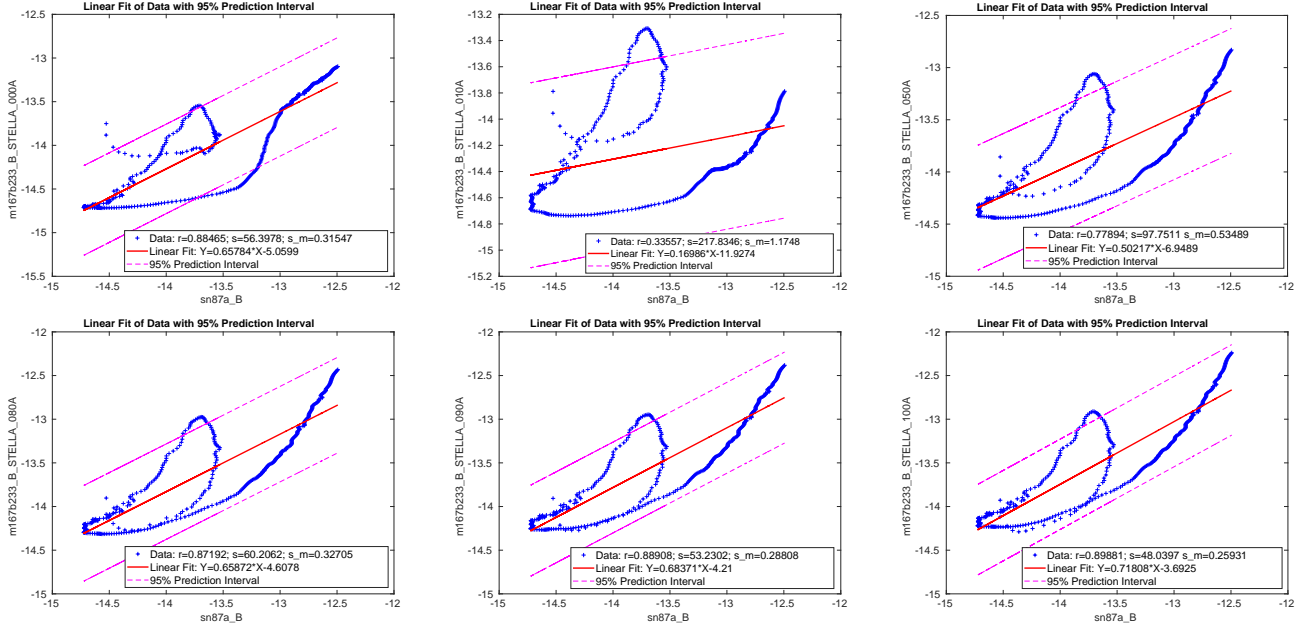


**Figure A3.** The  $B$ -band magnitudes for the 16-7b model computed with STELLA using different ratios between absorption and scattering, and observations of SN 1987A.

**Table A4.** The same as Table A1 for the 16-7b STELLA broad-band magnitudes and SN 1987A magnitudes.

		$A$	$r$	$s$	$s_m$
U_87A	U_STELLA_000A	0.06837	0.13050	317.80879	2.28892
U_87A	U_STELLA_010A	0.08695	0.13709	343.13217	2.44217
U_87A	U_STELLA_050A	0.76728	0.85858	73.76258	0.56205
U_87A	U_STELLA_080A	1.03185	0.91171	60.67765	0.43050
U_87A	U_STELLA_090A	1.08594	0.92123	60.80450	0.43279
U_87A	U_STELLA_100A	1.13518	0.92595	64.97415	0.46718
<hr/>					
B_87A	B_STELLA_000A	0.65784	0.88465	56.3978	0.31457
B_87A	B_STELLA_010A	0.16986	0.33557	217.8346	1.1748
B_87A	B_STELLA_050A	0.50217	0.77894	97.7511	0.53489
B_87A	B_STELLA_080A	0.65872	0.87192	60.2062	0.32705
B_87A	B_STELLA_090A	0.68371	0.88908	53.2302	0.28808
B_87A	B_STELLA_100A	0.71808	0.89881	48.0397	0.25931
<hr/>					
V_87A	V_STELLA_000A	0.79803	0.92585	35.4874	0.15782
V_87A	V_STELLA_010A	0.45557	0.74768	111.1707	0.50002
V_87A	V_STELLA_050A	0.58864	0.85189	72.5256	0.32627
V_87A	V_STELLA_080A	0.67421	0.90059	51.2285	0.22959
V_87A	V_STELLA_090A	0.68007	0.91032	47.8315	0.21402
V_87A	V_STELLA_100A	0.69792	0.91697	44.3254	0.19796
<hr/>					
R_87A	R_STELLA_000A	0.91404	0.92960	23.77577	0.09832
R_87A	R_STELLA_010A	0.82889	0.92540	24.76832	0.10066
R_87A	R_STELLA_050A	0.81238	0.92252	25.83081	0.10519
R_87A	R_STELLA_080A	0.84719	0.93368	22.09643	0.08996
R_87A	R_STELLA_090A	0.84185	0.93614	21.42282	0.08721
R_87A	R_STELLA_100A	0.84607	0.93794	20.83242	0.08481
<hr/>					
I_87A	I_STELLA_000A	0.99412	0.94056	20.47483	0.08229
I_87A	I_STELLA_010A	0.96658	0.96296	11.81486	0.04632
I_87A	I_STELLA_050A	0.88718	0.94229	17.80415	0.06965
I_87A	I_STELLA_080A	0.90315	0.94723	16.32774	0.06381
I_87A	I_STELLA_090A	0.90073	0.94690	16.42541	0.06422
I_87A	I_STELLA_100A	0.89997	0.94716	16.34396	0.06393



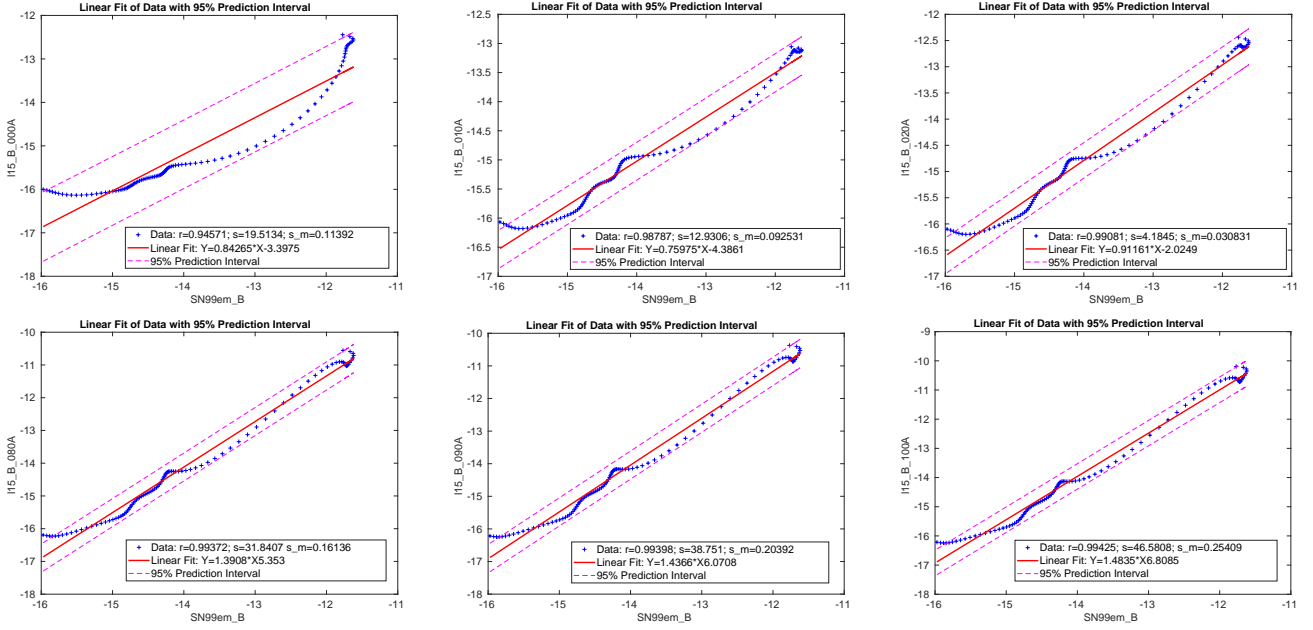


**Figure A4.** The  $B$ -band magnitudes for the L15 model computed with STELLA using different ratios between absorption and scattering, and observations of SN 1999em.

**Table A5.** The same as Table A1 for the L15 STELLA broad-band magnitudes and SN 1999em magnitudes.

		$A$	$r$	$s$	$s_m$
U_sn99em	U_STELLA_L15_000A	0.30067	0.97527	80.26059	0.44725
U_sn99em	U_STELLA_L15_010A	0.67449	0.98157	20.02893	0.13150
U_sn99em	U_STELLA_L15_020A	0.76093	0.97187	14.82002	0.09496
U_sn99em	U_STELLA_L15_080A	0.93246	0.98199	5.97510	0.03312
U_sn99em	U_STELLA_L15_090A	0.95300	0.98158	5.95111	0.03151
U_sn99em	U_STELLA_L15_100A	0.97224	0.98208	5.78599	0.02953
B_sn99em	B_STELLA_L15_000A	0.84265	0.94571	19.51341	0.11392
B_sn99em	B_STELLA_L15_010A	0.75975	0.98787	12.93062	0.09253
B_sn99em	B_STELLA_L15_020A	0.91161	0.99081	4.18450	0.03083
B_sn99em	B_STELLA_L15_080A	1.39078	0.99372	31.84070	0.16136
B_sn99em	B_STELLA_L15_090A	1.43664	0.99398	38.75098	0.20392
B_sn99em	B_STELLA_L15_100A	1.48351	0.99425	46.58084	0.25409
V_sn99em	V_STELLA_L15_000A	1.13095	0.98045	7.21903	0.02631
V_sn99em	V_STELLA_L15_010A	0.86758	0.98447	4.36066	0.02386
V_sn99em	V_STELLA_L15_020A	0.95116	0.98997	2.18841	0.01139
V_sn99em	V_STELLA_L15_080A	1.26760	0.99398	9.58007	0.03485
V_sn99em	V_STELLA_L15_090A	1.30034	0.99346	11.83005	0.04448
V_sn99em	V_STELLA_L15_100A	1.33826	0.99367	14.437937	0.05595